Editors' Suggestion

Simulating Holographic Conformal Field Theories on Hyperbolic Lattices

Santanu Dey,[1,2,*] Anffany Chen,[1,2,†] Pablo Basteiro,[3,4] Alexander Fritzsche,[3,4,5] Martin Greiter,[3,4] Matthias Kaminski,[6] Patrick M. Lenggenhager,[4,7,8,9,10] René Meyer,[3,4] Riccardo Sorbello,[3,4] Alexander Stegmaier,[3,4] Ronny Thomale,[3,4] Johanna Erdmenger,[3,4] and Igor Boettcher[1,2]

[1]*Department of Physics, University of Alberta, Edmonton, Alberta T6G 2E1, Canada*
[2]*Theoretical Physics Institute, University of Alberta, Edmonton, Alberta T6G 2E1, Canada*
[3]*Institute for Theoretical Physics and Astrophysics, Julius Maximilians University Würzburg, Am Hubland, 97074 Würzburg, Germany*
[4]*Würzburg-Dresden Excellence Cluster ct.qmat, Julius Maximilians University Würzburg, Am Hubland, 97074 Würzburg, Germany*
[5]*Institut für Physik, Universität Rostock, 18059 Rostock, Germany*
[6]*Department of Physics and Astronomy, University of Alabama, Tuscaloosa, Alabama 35487, USA*
[7]*Department of Physics, University of Zurich, 8057 Zurich, Switzerland*
[8]*Condensed Matter Theory Group, Paul Scherrer Institute, 5232 Villigen, Switzerland*
[9]*Institute for Theoretical Physics, ETH Zurich, 8093 Zurich, Switzerland*
[10]*Max Planck Institute for the Physics of Complex Systems, Nöthnitzer Strasse 38, 01187 Dresden, Germany*

(Received 3 April 2024; accepted 11 July 2024; published 9 August 2024)

We demonstrate how tabletop settings combining hyperbolic lattices with nonlinear dynamics universally encode aspects of the bulk-boundary correspondence between gravity in anti–de-Sitter (AdS) space and conformal field theory (CFT). Our concrete and broadly applicable holographic toy model simulates gravitational self-interactions in the bulk and features an emergent CFT with nontrivial correlations on the boundary. We measure the CFT data contained in the two- and three-point functions and clarify how a thermal CFT is simulated through an effective black hole geometry. As a concrete example, we propose and simulate an experimentally feasible protocol to measure the holographic CFT using electrical circuits.

DOI: 10.1103/PhysRevLett.133.061603

The holographic principle as realized by the AdS/CFT correspondence postulates a deep connection between two of the most intriguing, yet unfathomable phenomena in modern physics [1–4]: scale invariance close to second-order phase transitions, described by conformal field theories (CFTs) [5], and quantum gravity in curved spacetimes. The conjecture states that gravity in a negatively curved space is dual to a CFT on the boundary of that space. Furthermore, the presence of a black hole in the bulk results in a thermal CFT, with the temperature given by the Hawking temperature. While numerous calculations indicate the validity of the correspondence, an experimental verification is complicated in particular by the need to observe or simulate graviton-graviton interactions, since only these give rise to nonvanishing three- or four-point boundary correlation functions, and nontrivial CFT data.

The goal of this work is to construct a concrete holographic toy model for the AdS/CFT correspondence that can be realized in the laboratory. We show that, with the right four ingredients, a large class of realistic and experimentally feasible low-energy models features holography through conformal boundary correlations. As a concrete example, we demonstrate how electrical circuits with nonlinear circuit elements can achieve this milestone, but our universal model is applicable to other experimental platforms and constitutes a theoretically intriguing model in itself. With the setup, we are able to emulate three-point functions, characterize the CFT data, and clarify how thermal effects are incorporated.

The four ingredients of our holographic toy model are (i) a lattice realization of anti–de-Sitter (AdS) space through hyperbolic lattices [6–49], now routinely implemented in circuit quantum electrodynamics and coplanar waveguides [6,50], topoelectrical circuits [20,23,29,30], topological photonics [51], and mechanical elastic lattices [52]; (ii) nonlinear dynamical equations to emulate gravitational self-interactions, realized by local qubit-photon interactions [16,53,54], nonlinear or active circuit elements [55–59], nonlinear optics [60,61], or spring hardening; (iii) effective black hole geometries to emulate temperature by using type-II hyperbolic lattices [35,62–64]; (iv) a theoretical framework and experimental protocol to compute and measure boundary correlation functions. We demonstrate that with (i)–(iv) even classical platforms are holographic, corresponding to the limit where weakly

*Contact author: santanu@ualberta.ca
†Contact author: anffany@ualberta.ca

coupled semiclassical bulk gravity is dual to a strongly coupled CFT, as reviewed in [4].

Our work considerably extends previous works on holographic aspects of hyperbolic lattices. Power-law scaling of two-point boundary correlators has been demonstrated at zero temperature in the important works [10,13,35], together with the massless contact limit of the four-point function [13], the introduction of black holes through type-II lattices [35], and the emergence of the Ryu-Takayanagi formula [35]. However, our systematic study of higher-point correlation functions and their ensuing CFT data, precise characterization of thermal correlations, theoretical framework and concrete experimental protocol to measure boundary correlations, and simulation of an experimental setup satisfying (i)–(iv) is unprecedented. This is critical for a thorough investigation of both the duality, and consistency of the associated CFT. Here we achieve this milestone for the first time by studying interacting hyperbolic matter on the lattice.

Holographic lattice model—Classical or quantum theories of gravity are models where the metric tensor g and distance line element $\mathrm{d}s^2 = \sum_{\alpha,\beta} g_{\alpha\beta}\mathrm{d}x^\alpha \mathrm{d}x^\beta$ fluctuate in time and space. In two imaginary-time spacetime dimensions, the metric can be parametrized by a single real field $\varphi(z)$ as $\mathrm{d}s^2 = e^{\varphi(z)}|\mathrm{d}z|^2$ (isothermal coordinates), where $z = x + \mathrm{i}y$. Although the usual Einstein-Hilbert action is nondynamical in two dimensions, a dynamical action principle for gravity results from minimizing the Liouville gravity action [65,66]

$$S_{\mathrm{LG}}[\varphi] = \int \mathrm{d}^2 z \left[\frac{1}{2}(\nabla\varphi)^2 + \frac{2}{\ell^2}e^{\varphi}\right]. \tag{1}$$

The term $-1/\ell^2$ plays the role of a negative cosmological constant. The stationary solution $\varphi_\star(z)$ that minimizes the action is the hyperbolic Poincaré disk metric $\mathrm{d}s^2_\star = (2\ell)^2|\mathrm{d}z|^2/(1-|z|^2)^2$. Fluctuations about this solution, $\varphi = \varphi_\star + \phi$, follow the imaginary-time action [67]

$$\begin{aligned} S_{\mathrm{grav}}[\phi] &= S_{\mathrm{LG}}[\varphi_\star + \phi] - S_{\mathrm{LG}}[\varphi_\star] \\ &= \int \frac{\mathrm{d}^2 z}{(1-|z|^2)^2}\left[\frac{1}{2}\phi(-\Box + m^2)\phi + \frac{\phi^3}{3\ell^2} + \frac{\phi^4}{12\ell^2} + \ldots\right]. \end{aligned} \tag{2}$$

We may interpret $\phi(z)$ as a gravitonlike mode, since it parametrizes small metric fluctuations. Importantly, dynamical gravity corresponds here to a real scalar field ϕ propagating in its own hyperbolic background with $\Box = (2\ell)^{-2}(1-|z|^2)^2\nabla^2$ the Laplace-Beltrami operator [ingredient (i)], and nonlinear terms like ϕ^3 and ϕ^4 correspond to gravitational self-interactions [ingredient (ii)]. We choose $m^2\ell^2 > -1/4$ above the Breitenlohner-Freedman bound for a stable theory [33].

The continuum action (2) can be simulated on discrete hyperbolic lattices using the dictionary of Ref. [11], which yields the universal holographic lattice action

$$S(\{\phi_\mu\}) = -\frac{1}{2}\sum_{\mu,\nu}\phi_\mu A_{\mu\nu}\phi_\nu + \sum_\mu\left(\frac{\hat{m}^2}{2}\phi_\mu^2 + \frac{u}{3!}\phi_\mu^3\right). \tag{3}$$

Herein, $\phi_\mu = \phi(z_\mu)$ is the field variable defined on the sites z_μ of a graph or lattice $\mathcal{G}$ with adjacency matrix A. Equation (3) represents a generic tight-binding Hamiltonian realizable on the platforms discussed in the introduction, and is a universal low-energy limit of more complicated Hamiltonians. The parameters $\hat{m}^2$ and u are tunable in experiment and can be matched to the Liouville action (1) [67]. We neglect higher-order interaction terms beyond ϕ^3 for simplicity, resulting in a model that deviates from Liouville gravity through this omission.

The choice of graph $\mathcal{G}$ determines the curved bulk space on which the action is simulated. Two-dimensional imaginary-time AdS space is emulated by hyperbolic $\{p, q\}$ lattices with $(p-2)(q-2) > 4$, labeled type-I hereafter. Black holes are realized by identifying points on two geodesics in a type-I geometry. This is equivalent to a type-II ring graph [35] obtained by a squash-and-wrap procedure, see Fig. 1. The squash step is $z_\mu \mapsto \zeta_\mu = (2/\pi)\ln[(1+z_\mu)/(1-z_\mu)]$, which produces an infinite strip, from which a finite strip of width w is obtained with its truncated edges identified, followed by the wrap step $\zeta_\mu \mapsto \hat{z}_\mu = e^{2\pi\mathrm{i}(\zeta_\mu+\mathrm{i})/w}$ yielding a ring. When applied to the Poincaré disk metric, this results in a time slice of the three-dimensional Bañados-Teitelboim-Zanelli (BTZ) black hole metric [35,62–64,67] given by

$$\mathrm{d}s^2_{\mathrm{II}} = \left(\frac{\ell w}{4}\right)^2 \frac{|\mathrm{d}\hat{z}|^2}{|\hat{z}|^2\cos^2[\frac{\pi}{2}(1-\ln|\hat{z}|/\ln\hat{r}_{\mathrm{H}})]}, \tag{4}$$

which suggests the black hole interpretation on the lattice. The black hole temperature is $T = w/8\pi\ell$ with horizon radius $\hat{r}_{\mathrm{H}} = e^{-2\pi/w}$. In our numerical construction [67], we have $w = kP$, where k is an integer that we can choose freely and $P = P(p,q)$ is a lattice-dependent constant. By varying k, p, q, we can access a large, albeit discrete set of temperatures [ingredient (iii)].

Bulk-boundary correspondence—To study holography, we divide the graph $\mathcal{G}$, which may be either type-I or type-II, into its bulk and boundary components, $\mathring{\mathcal{G}}$ and $\partial\mathcal{G}$, such that $\mathcal{G} = \mathring{\mathcal{G}} \cup \partial\mathcal{G}$. We label generic sites on $\mathcal{G}$ by Greek letters μ, ν, whereas bulk and boundary sites are labeled by Roman letters i, j and a, b, respectively. We then consider fixed boundary field values given by $\phi_a = J_a$. The associated bulk partition function reads

$$Z(\{J_a\}) = \int\left(\prod_i \mathrm{d}\phi_i\right) e^{-S(\{\phi_i,\phi_a=J_a\})}. \tag{5}$$

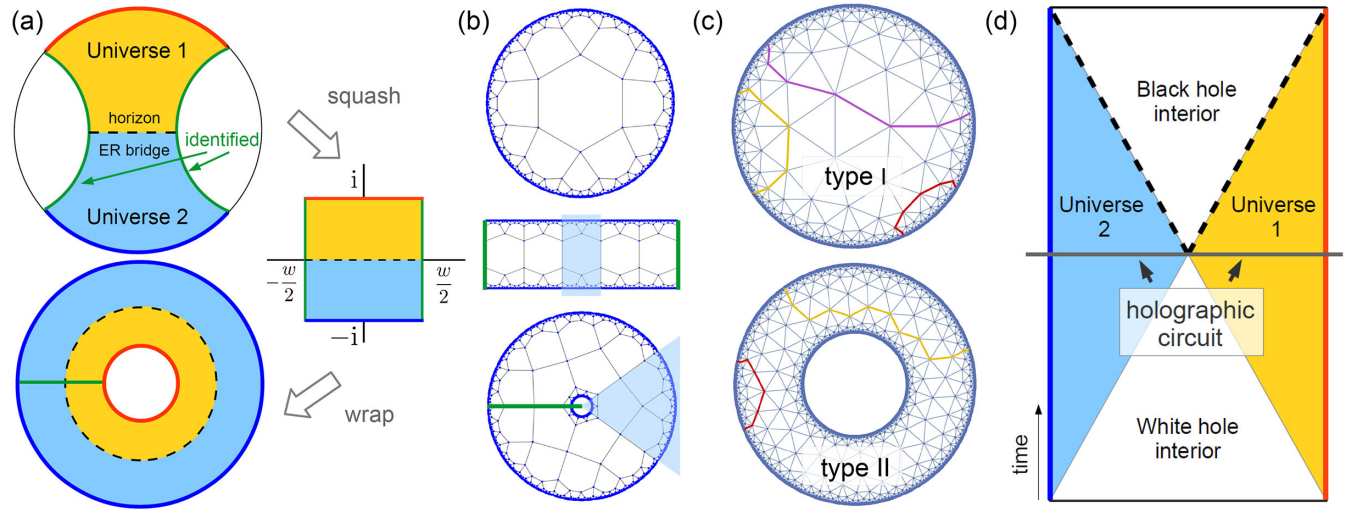

FIG. 1. Hyperbolic flakes and black hole geometry. (a) Starting from a Poincaré disk (type-I geometry, coordinates $z = re^{i\theta}$), we create a black hole by identifying points on two geodesics (shown in green). Equivalently, we squash the disk to form a strip of width w and then wrap it into a ring (type-II geometry, coordinates $\hat{z} = \hat{r}e^{i\theta}$). This identification creates two separate Universes, 1 and 2, each with a holographic boundary, connected through an Einstein-Rosen (ER) bridge (dashed line) [68]. This line corresponds to the bifurcation point of an eternal black hole horizon. (b) Applying the squash-and-wrap procedure to a hyperbolic $\{p, q\}$ flake creates a type-II flake, which emulates a black hole with Hawking temperature $T = w/8\pi\ell$. Herein, $w = kP$, with k an integer representing the number of repeated cells in the strip ($k = 5$ in the plot), and $P = P(p, q)$ a constant. (c) Type-I and -II hyperbolic flakes of a $\{3, 7\}$ tessellation with some graph-shortest-distance paths connecting boundary sites. These paths are pivotal for the boundary-boundary correlations. (d) Schematic Penrose diagram with space and time as the x axis and y axis, respectively. The hyperbolic lattice is located on a slice of constant time (gray line).

Note that we only integrate over the bulk field values. The bulk-boundary correspondence asserts that $Z(\{J_a\})$ is the generating function for a CFT on the boundary [2,3]. The associated connected n-point correlation functions for some boundary field $\mathcal{O}_a$ are given by

$$\langle \mathcal{O}_{a_1}, \ldots, \mathcal{O}_{a_n} \rangle = \left. \frac{\partial^n \ln Z}{\partial J_{a_1} \cdots \partial J_{a_n}} \right|_{J=0} \tag{6}$$

[ingredient (iv)]. Properties like spin or scaling behavior of $\mathcal{O}_a$ are determined by the bulk theory, but no action underlying the CFT is specified by the duality *per se*. An important future research inquiry is to explore whether a representative CFT action can be constructed in the holographic toy model. Furthermore, adding more fields and symmetries to the bulk action, the consistency of richer dual CFTs can be probed.

The holographic properties of the lattice model (3) can be studied theoretically in the perturbative regime $u \ll 1$, which mirrors the semiclassical limit of the AdS/CFT correspondence where only tree-level diagrams contribute [67]. The two-point function for $u = 0$ reads

$$\langle \mathcal{O}_a \mathcal{O}_b \rangle = -M_{ab} + \sum_{i,j} M_{ai} G_{ij} M_{jb}. \tag{7}$$

Here, $M_{\mu\nu} = (G^{-1})_{\mu\nu} = -A_{\mu\nu} + \hat{m}^2 \delta_{\mu\nu}$ is the bare inverse propagator, with $\hat{m}^2 = q + qh^2 m^2 \ell^2$ relating to the physical mass m through a dimensionless lattice constant $h = \{1 - [\sin^2(\pi/q)/\cos^2(\pi/p)]\}^{1/2}$ [11,38]. Approximately, $\langle \mathcal{O}_a \mathcal{O}_b \rangle \approx G_{ab}$ is the bulk propagator extrapolated to the boundary sites a, b. For the three-point function, we have

$$\langle \mathcal{O}_a \mathcal{O}_b \mathcal{O}_c \rangle = u \sum_i B_{ai} B_{bi} B_{ci} \tag{8}$$

with $B_{ai} = \sum_j M_{aj} G_{ji}$ the boundary-to-bulk propagator. This is a Witten diagram, where the bulk site i connects the boundary sites a, b, c, see Fig. 3(a), and the largest contribution comes from graph-geodesic paths. Remarkably, this perturbative formula captures the CFT correlations also on the lattice. All n-point functions with $n \geq 3$ vanish for $u = 0$ in our model, emphasizing again the importance of interactions embodied by $u\phi^3$ in Eq. (3). A four-point function appears at order u^2 [4].

Correlation functions and CFT data—The characteristic forms of the two- and higher-point correlation functions of a CFT distinguish it from a mere scale invariant theory. In particular, the two- and three-point functions are fully determined by two parameters as part of their CFT data, the scaling dimension Δ and three-point coefficient C_3,

$$\langle \mathcal{O}_a \mathcal{O}_b \rangle \simeq \frac{1}{(d_{ab})^{2\Delta}}, \quad \langle \mathcal{O}_a \mathcal{O}_b \mathcal{O}_c \rangle \simeq \frac{C_3}{(d_{ab} d_{ac} d_{bc})^{\Delta}}. \tag{9}$$

Here we normalize the boundary fields $\mathcal{O}_a$ such that the numerator of the two-point function is unity. The function d_{ab} determines the distance between the sites a, b in the CFT. A hallmark of the continuum AdS/CFT correspondence is that Δ and C_3 are tunable by varying the bulk parameters $m^2\ell^2$ and u. We now show that the same is true for our holographic lattice model.

The boundary two- and three-point functions determined from Eqs. (7) and (8) are summarized in Figs. 2 and 3, respectively. They agree with the expected behavior through the identification [67]

$$d_{ab} = \begin{cases} |e^{i\theta_a} - e^{i\theta_b}| & \text{(type-I)} \\ \frac{\sinh(\pi T\ell|\theta_a - \theta_b|)}{\pi T\ell} & \text{(type-II)} \end{cases}. \tag{10}$$

Here $\theta_{a,b}$ are the angle coordinates of the boundary sites. This emulates CFTs on a circle at zero and finite temperature. While Eqs. (9) are good approximations on type-II lattices, especially for the two-point function, the proper quantitative formula requires to replace $\theta_a - \theta_b \to \theta_a - \theta_b + 2\pi n$ in d_{ab} with a subsequent sum over $n \in \mathbb{Z}$ to make the functions periodic [67]. This behavior, reminiscent of the method of images, also arises in the BTZ geometry and is thus expected here [64].

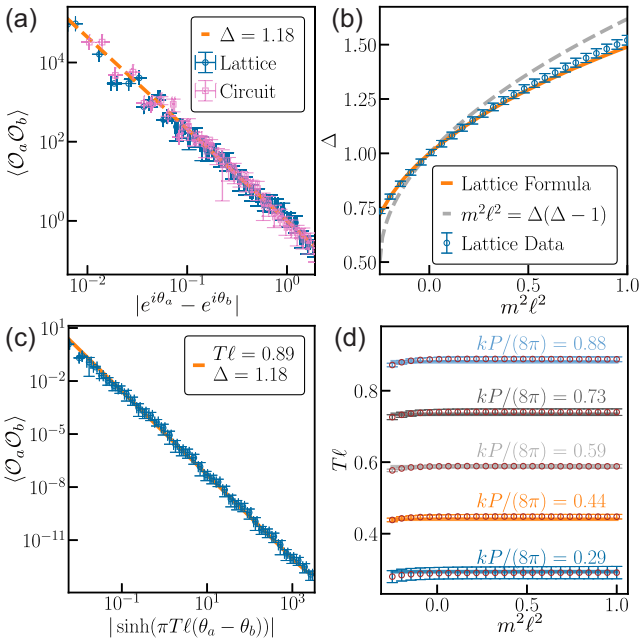

FIG. 2. CFT two-point function. Results are shown for {3,7} hyperbolic flakes. (a) Representative two-point function in type-I geometry with bulk mass $m^2\ell^2 = 0.271$. Datasets are computed from Eq. (7) (blue) and numerical simulation of the electrical circuit in Eqs. (12)–(14) using a realistic diode (pink). The data scatter results from binning the discrete lattice coordinates θ_a. Fitted power-law formula (9) shown in orange. (b) Fitted conformal dimension Δ versus $m^2\ell^2 > -1/4$ (blue squares with fit error). Because of lattice corrections captured by Eq. (11) (orange), Δ deviates from the continuum formula $m^2\ell^2 = \Delta(\Delta - 1)$ (gray dashed). (c) Two-point function on the type-II lattice for the same mass as in **a**, showing thermal behavior according to Eq. (9). (d) The fitted type-II temperature T (circles) is approximately independent of m and described by $T\ell = kP/8\pi$ (lines). Here, $P \approx 1.845$ for {3,7} and $k = 4$, 6, 8, 10, 12 in the plot.

Our main novel findings from the analysis of correlations are that (1) the scaling dimension $\Delta(m^2\ell^2)$ extracted from the two-point function also captures the scaling of the three-point function, indicating a consistent CFT [Fig 3(d)], (2) the parameter k on type-II lattices determines the temperature consistent with the formula $T\ell = kP/8\pi$ [Fig. 2(d)], but leaves the CFT data invariant, and (3) the CFT data $\Delta(m^2\ell^2)$ and $C_3(m^2\ell^2)$ for the CFTs simulated on both type-I and type-II lattices are identical [Figs. 3(d) and 3(e)]. The latter finding indicates that they are the same CFTs, but at zero and finite temperature. These nontrivial results also solidify the interpretation of the type-II lattice as a geometry that emulates a black hole.

The holographic relation between Δ and $m^2\ell^2$ is of the form $m^2\ell^2 = f[\Delta(\Delta - 1)]$ with $f_{\text{cont}}(X) = X$ in the continuum, while a gradient expansion for the {3,7} lattice yields

$$f(X) \simeq X + \frac{h^2}{4}(X^2 + 2X) + \frac{h^4}{36}(X^3 + 10X^2 + 12X) \tag{11}$$

with $h = 0.497$ [19,22,67], see Fig. 2(b). The value of h and form of $f(X)$ depend on the $\{p, q\}$ lattice, with the universal continuum limit recovered for $h \to 0$. To extract the three-point coefficient C_3 in a manner that reduces scatter due to the lattice discretization, we construct the function $F_{abc} = \langle \mathcal{O}_a \mathcal{O}_b \mathcal{O}_c \rangle / [\langle \mathcal{O}_a \mathcal{O}_b \rangle \langle \mathcal{O}_a \mathcal{O}_c \rangle \langle \mathcal{O}_b \mathcal{O}_c \rangle]^{1/2}$ that we average over a, b, c to obtain $F_{abc} \simeq C_3$ [67].

Experimental protocol for electrical circuits—We propose to realize the holographic toy model in electrical circuits by implementing the equation of motion

$$-\sum_\nu A_{\mu\nu} \bar{V}_\nu + \hat{m}^2 \bar{V}_\mu + \frac{u}{2} \bar{V}_\mu^2 = 0, \tag{12}$$

where $\phi_\mu \to \bar{V}_\mu$ is the normalized local voltage at node z_μ. By applying voltage sources on the boundary, fixed values $\bar{V}_a = J_a$ can be realized. The solution $\bar{V}_\mu$ parametrically depends on the J_a chosen. By applying time-dependent boundary conditions, $J_a(t)$, t derivatives conveniently translate to J_a derivatives below. From the measured or simulated voltage signal $\bar{V}_\mu(t)$, we compute the circuit generating function

$$W_{\text{circ}}(t) = -S(\{\bar{V}_\mu(t)\}), \tag{13}$$

with action $S(\{\phi_\mu\})$ from Eq. (3). We have $W_{\text{circ}} \simeq \ln Z$ in the saddle-point approximation, sufficient for the semiclassical holographic limit studied here.

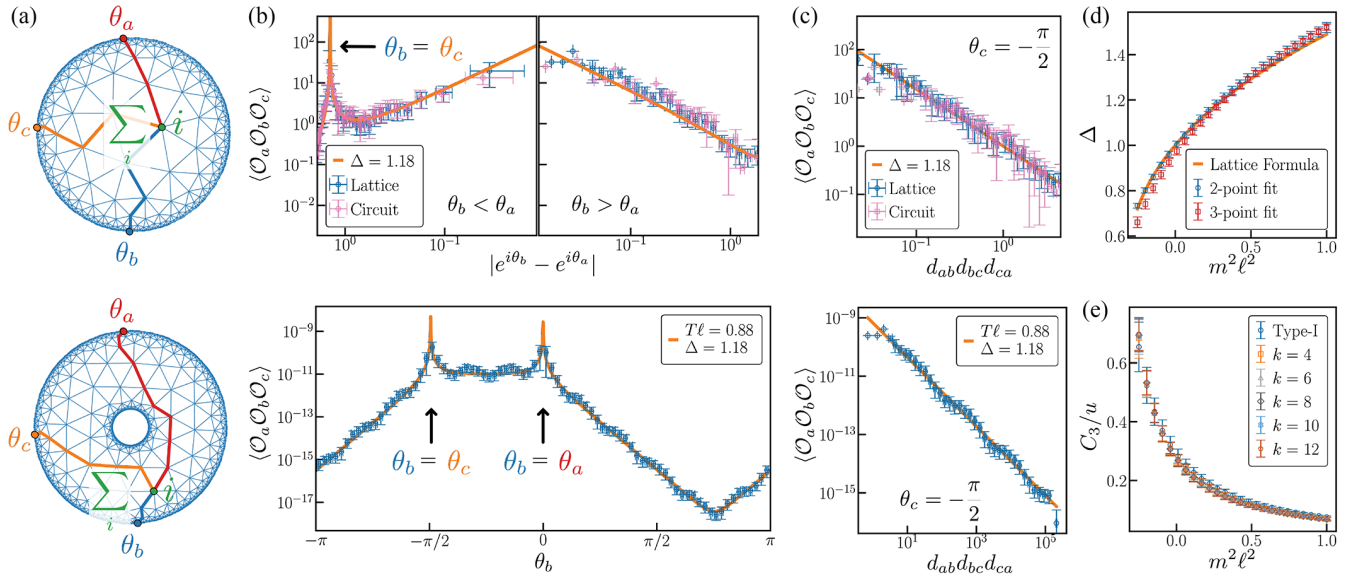

FIG. 3. CFT three-point function. We visualize the three-point function on type-I (top row) and type-II geometries (bottom row). We place $\mathcal{O}_a$ at angle θ_a, $\mathcal{O}_c$ at angle θ_c, and vary the position of $\mathcal{O}_b$ at angle θ_b. (a) The three-point function corresponds to the star-shaped Witten diagram of Eq. (8). The largest contribution to the sum comes from graph-geodesic paths connecting the boundary sites through an intermediate bulk site i. (b) Three-point functions on {3,7} type-I and type-II flakes with parameters as in Fig. 2. Datasets are computed from Eq. (8) (blue) and numerical simulation of the electrical circuit in Eqs. (12)–(14) using a realistic diode (pink). The solid orange lines constitute the theory prediction, where Δ and T follow from the two-point function, and only C_3 is a fitted parameter. Correlations diverge when any two of the angles coincide (arrows). (c) Scaling collapse according to the characteristic power-law behavior $\langle \mathcal{O}_a\mathcal{O}_b\mathcal{O}_c\rangle \propto (d_{ab}d_{ac}d_{bc})^{-\Delta}$ (orange), where $d_{ab} = |e^{i\theta_a} - e^{i\theta_b}|$ for type-I and $d_{ab}(T) = \sinh(\pi T\ell|\theta_a - \theta_b|)/\pi T\ell$ for type-II geometries, respectively. (d) Scaling dimensions $\Delta(m^2\ell^2)$ extracted from two- and three-point function on type-I graphs are consistent within the errors. (e) The normalized three-point coefficient C_3/u is determined by $m^2\ell^2$ and agrees for both type-I and type-II lattices, indicating their CFTs are equal.

To realize the terms in Eq. (12), we use resistors to generate the linear couplings $\sum_\nu(-A_{\mu\nu} + \hat{m}^2\delta_{\mu\nu})V_\nu$, while diodes can be used for the nonlinear term uV_μ^2. Indeed, the current through a diode is approximated by the Shockley equation $I(V) = I_S(e^{V/V_S} - 1) \approx I_S[V/V_S + (V/V_S)^2/2]$, which yields the desired V_μ^2 term after absorbing the linear part into $\hat{m}^2V_\mu$. The concrete circuit parameters are listed in Supplemental Sec. S8 [67]. On short timescales, dissipative terms present in any realistic circuit lead to transient behavior. These effects are neglected here and the correspondence is realized in the steady state, assuming an instantaneous response to $J_a(t)$.

Our protocol to compute two-point functions from $W_{\mathrm{circ}}(t)$ is as follows. We apply a drive that linearly ramps $J_{a,b}(t) = K_{a,b} \times (t - t_0)$, crossing zero at $t = t_0$, while all other $J_\mu(t) \equiv 0$ for $\mu \neq a$, b. Since all second time derivatives vanish, we have

$$\left.\frac{\mathrm{d}^2W_{\mathrm{circ}}}{\mathrm{d}t^2}\right|_{t=t_0} = \sum_{\mu,\nu}\dot{J}_\mu\dot{J}_\nu\left.\frac{\partial^2W_{\mathrm{circ}}}{\partial J_\mu\partial J_\nu}\right|_{J=0} = K_a^2\langle\mathcal{O}_a^2\rangle + 2K_aK_b\langle\mathcal{O}_a\mathcal{O}_b\rangle + K_b^2\langle\mathcal{O}_b^2\rangle. \quad (14)$$

By choosing three linearly independent ramps in a series of measurements, e.g., $(K_a, K_b) = (1,0), (0,1), (1,1)$, this set of three linear equations can be solved for $\langle\mathcal{O}_a\mathcal{O}_b\rangle$. Similarly, to measure n-point functions, we ramp n boundary sites $J_{a_1}(t), \ldots, J_{a_n}(t)$ linearly. By using ten linearly independent ramps, we obtain $\langle\mathcal{O}_a\mathcal{O}_b\mathcal{O}_c\rangle$ from $\mathrm{d}^3W_{\mathrm{circ}}/\mathrm{d}t^3|_{t=t_0}$.

In Fig. 2(a) we present results for the so-obtained two-point function using an LTspice simulation of an electrical circuit with a realistic Schottky diode (model RBE1VAM20A). In Figs. 3(b) and 3(c) we present the three-point function for the same parameters from a *Mathematica* simulation of Eqs. (12)–(14). Since the signals in actual electrical circuits are known to be close to such numerical simulations [55–57], this serves as a proof of principle that our protocol is experimentally feasible.

Acknowledgments—We thank Joseph Maciejko for profound contributions especially in the early stages of the project and his insightful comments on the manuscript. We are grateful for fruitful discussions with Giuseppe Di Giulio, Dominik Neuenfeld, and Canon Sun. A. C. was supported by the Natural Sciences and Engineering Research Council of Canada (NSERC) Discovery Grant No. RGPIN-2020-06999, the Avadh Bhatia Fellowship, and the Faculty of Science at the University of Alberta. A. C. and I. B. acknowledge support through the University

of Alberta startup fund UOFAB Startup Boettcher. S. D. was supported by the Faculty of Science at the University of Alberta. M. K. was supported, in part, by the U.S. Department of Energy Grant No. DE-SC0012447. I. B. acknowledges funding from the NSERC Discovery Grants No. RGPIN-2021-02534 and No. DGECR2021-00043. P. B., A. F., M. G., P. M. L., R. M., R. S., A. S., R. T., and J. E. acknowledge support by Germany's Excellence Strategy through the Würzburg-Dresden Cluster of Excellence on Complexity and Topology in Quantum Matter—ct.qmat (EXC 2147, project-id 390858490), and by the Deutsche Forschungsgemeinschaft (DFG) through the Collaborative Research Center "ToCoTronics," Project-ID 258499086—SFB 1170. P. M. L. was supported by the Ambizione Grant No. 185806 by the Swiss National Science Foundation (SNSF) and the European Union (ERC, QuSimCtrl, 101113633). Views and opinions expressed are however those of the authors only and do not necessarily reflect those of the European Union or the European Research Council Executive Agency. Neither the European Union nor the granting authority can be held responsible for them.

S. D. and A. C. contributed equally to this letter.

[1] J. Maldacena, The large-N limit of superconformal field theories and supergravity, Int. J. Theor. Phys. **38**, 1113 (1999).
[2] E. Witten, Anti de Sitter space and holography, Adv. Theor. Math. Phys. **2**, 253 (1998).
[3] S. S. Gubser, I. R. Klebanov, and A. M. Polyakov, Gauge theory correlators from noncritical string theory, Phys. Lett. B **428**, 105 (1998).
[4] M. Ammon and J. Erdmenger, *Gauge/Gravity Duality: Foundations and Applications* (Cambridge University Press, Cambridge, England, 2015), 10.1017/CBO9780511846373.
[5] P. Di Francesco, P. Mathieu, and D. Senechal, *Conformal Field Theory*, Graduate Texts in Contemporary Physics (Springer-Verlag, New York, 1997), 10.1007/978-1-4612-2256-9.
[6] A. J. Kollár, M. Fitzpatrick, and A. A. Houck, Hyperbolic lattices in circuit quantum electrodynamics, Nature (London) **571**, 45 (2019).
[7] A. J. Kollár, M. Fitzpatrick, P. Sarnak, and A. A. Houck, Line-graph lattices: Euclidean and non-Euclidean flat bands, and implementations in circuit quantum electrodynamics, Commun. Math. Phys. **376**, 1909 (2020).
[8] L. Boyle, M. Dickens, and F. Flicker, Conformal quasicrystals and holography, Phys. Rev. X **10**, 011009 (2020).
[9] S. Yu, X. Piao, and N. Park, Topological hyperbolic lattices, Phys. Rev. Lett. **125**, 053901 (2020).
[10] M. Asaduzzaman, S. Catterall, J. Hubisz, R. Nelson, and J. Unmuth-Yockey, Holography on tessellations of hyperbolic space, Phys. Rev. D **102**, 034511 (2020).
[11] I. Boettcher, P. Bienias, R. Belyansky, A. J. Kollár, and A. V. Gorshkov, Quantum simulation of hyperbolic space with circuit quantum electrodynamics: From graphs to geometry, Phys. Rev. A **102**, 032208 (2020).
[12] A. Jahn, Z. Zimborás, and J. Eisert, Central charges of aperiodic holographic tensor-network models, Phys. Rev. A **102**, 042407 (2020).
[13] R. C. Brower, C. V. Cogburn, A. L. Fitzpatrick, D. Howarth, and C.-I. Tan, Lattice setup for quantum field theory in AdS_2, Phys. Rev. D **103**, 094507 (2021).
[14] X. Zhu, J. Guo, N. P. Breuckmann, H. Guo, and S. Feng, Quantum phase transitions of interacting bosons on hyperbolic lattices, J. Phys. Condens. Matter **33**, 335602 (2021).
[15] J. Maciejko and S. Rayan, Hyperbolic band theory, Sci. Adv. **7**, eabe9170 (2021).
[16] P. Bienias, I. Boettcher, R. Belyansky, A. J. Kollar, and A. V. Gorshkov, Circuit quantum electrodynamics in hyperbolic space: From photon bound states to frustrated spin models, Phys. Rev. Lett. **128**, 013601 (2022).
[17] J. Maciejko and S. Rayan, Automorphic Bloch theorems for hyperbolic lattices, Proc. Natl. Acad. Sci. U.S.A. **119**, e2116869119 (2022).
[18] I. Boettcher, A. V. Gorshkov, A. J. Kollár, J. Maciejko, S. Rayan, and R. Thomale, Crystallography of hyperbolic lattices, Phys. Rev. B **105**, 125118 (2022).
[19] A. Stegmaier, L. K. Upreti, R. Thomale, and I. Boettcher, Universality of hofstadter butterflies on hyperbolic lattices, Phys. Rev. Lett. **128**, 166402 (2022).
[20] W. Zhang, H. Yuan, N. Sun, H. Sun, and X. Zhang, Observation of novel topological states in hyperbolic lattices, Nat. Commun. **13**, 2937 (2022).
[21] Z.-R. Liu, C.-B. Hua, T. Peng, and B. Zhou, Chern insulator in a hyperbolic lattice, Phys. Rev. B **105**, 245301 (2022).
[22] R. C. Brower, C. V. Cogburn, and E. Owen, Hyperbolic lattice for scalar field theory in AdS_3, Phys. Rev. D **105**, 114503 (2022).
[23] P. M. Lenggenhager, A. Stegmaier, L. K. Upreti, T. Hofmann, T. Helbig, A. Vollhardt, M. Greiter, C. H. Lee, S. Imhof, H. Brand, T. Kiesling, I. Boettcher, T. Neupert, R. Thomale, and T. Bzdusek, Simulating hyperbolic space on a circuit board, Nat. Commun. **13**, 4373 (2022).
[24] N. Cheng, F. Serafin, J. McInerney, Z. Rocklin, K. Sun, and X. Mao, Band theory and boundary modes of high-dimensional representations of infinite hyperbolic lattices, Phys. Rev. Lett. **129**, 088002 (2022).
[25] A. Attar and I. Boettcher, Selberg trace formula in hyperbolic band theory, Phys. Rev. E **106**, 034114 (2022).
[26] T. Bzdusek and J. Maciejko, Flat bands and band-touching from real-space topology in hyperbolic lattices, Phys. Rev. B **106**, 155146 (2022).
[27] P. Basteiro, G. D. Giulio, J. Erdmenger, J. Karl, R. Meyer, and Z.-Y. Xian, Towards explicit discrete holography: Aperiodic spin chains from hyperbolic tilings, SciPost Phys. **13**, 103 (2022).
[28] D. M. Urwyler, P. M. Lenggenhager, I. Boettcher, R. Thomale, T. Neupert, and T. Bzdusek, Hyperbolic topological band insulators, Phys. Rev. Lett. **129**, 246402 (2022).
[29] A. Chen, H. Brand, T. Helbig, T. Hofmann, S. Imhof, A. Fritzsche, T. Kießling, A. Stegmaier, L. K. Upreti, T. Neupert, T. Bzdusek, M. Greiter, R. Thomale, and I. Boettcher, Hyperbolic matter in electrical circuits with tunable complex phases, Nat. Commun. **14**, 622 (2023).

[30] W. Zhang, F. Di, X. Zheng, H. Sun, and X. Zhang, Hyperbolic band topology with non-trivial second Chern numbers, Nat. Commun. **14**, 1083 (2023).
[31] N. Gluscevich, A. Samanta, S. Manna, and B. Roy, Dynamic mass generation on two-dimensional electronic hyperbolic lattices, arXiv:2302.04864.
[32] Z.-R. Liu, C.-B. Hua, T. Peng, R. Chen, and B. Zhou, Higher-order topological insulators in hyperbolic lattices, Phys. Rev. B **107**, 125302 (2023).
[33] P. Basteiro, F. Dusel, J. Erdmenger, D. Herdt, H. Hinrichsen, R. Meyer, and M. Schrauth, Breitenlohner-Freedman bound on hyperbolic tilings, Phys. Rev. Lett. **130**, 091604 (2023).
[34] Q. Pei, H. Yuan, W. Zhang, and X. Zhang, Engineering boundary-dominated topological states in defective hyperbolic lattices, Phys. Rev. B **107**, 165145 (2023).
[35] J. Chen, F. Chen, Y. Yang, L. Yang, Z. Chen, Y. Meng, B. Yan, X. Xi, Z. Zhu, G.-G. Liu, P. P. Shum, H. Chen, R.-G. Cai, R.-Q. Yang, Y. Yang, and Z. Gao, AdS/CFT correspondence in hyperbolic lattices, arXiv:2305.04862.
[36] Y.-L. Tao and Y. Xu, Higher-order topological hyperbolic lattices, Phys. Rev. B **107**, 184201 (2023).
[37] N. Gluscevich and B. Roy, Magnetic catalysis in weakly interacting hyperbolic Dirac materials, arXiv:2305.11174.
[38] E. Petermann and H. Hinrichsen, Eigenmodes of the Laplacian on hyperbolic lattices, Phys. Rev. D **109**, 106019 (2024).
[39] R. Mosseri and J. Vidal, Density of states of tight-binding models in the hyperbolic plane, Phys. Rev. B **108**, 035154 (2023).
[40] A. Chen, Y. Guan, P. M. Lenggenhager, J. Maciejko, I. Boettcher, and T. Bzdušek, Symmetry and topology of hyperbolic Haldane models, Phys. Rev. B **108**, 085114 (2023).
[41] J. B. Curtis, P. Narang, and V. Galitski, Absence of weak localization on negative curvature surfaces, arXiv:2308.01351.
[42] G. Shankar and J. Maciejko, Hyperbolic lattices and two-dimensional Yang-Mills theory, arXiv:2309.03857.
[43] M. Schrauth, Y. Thurn, F. Goth, J. S. Portela, D. Herdt, and F. Dusel, Hypertiling–a high performance Python library for the generation and visualization of hyperbolic lattices, arXiv:2309.10844.
[44] A. Chen, J. Maciejko, and I. Boettcher, Anderson localization transition in disordered hyperbolic lattices, Phys. Rev. Lett. **133**, 066101 (2024).
[45] P. M. Lenggenhager, J. Maciejko, and T. Bzdusek, Non-Abelian hyperbolic band theory from supercells, Phys. Rev. Lett. **131**, 226401 (2023).
[46] T. Li, Y. Peng, Y. Wang, and H. Hu, Anderson transition and mobility edges on hyperbolic lattices, arXiv:2312.11857.
[47] P. Basteiro, R. N. Das, G. D. Giulio, and J. Erdmenger, Aperiodic spin chains at the boundary of hyperbolic tilings, SciPost Phys. **15**, 218 (2023).
[48] H. Yuan, W. Zhang, Q. Pei, and X. Zhang, Hyperbolic topological flat bands, Phys. Rev. B **109**, L041109 (2024).
[49] T. Tummuru, A. Chen, P. M. Lenggenhager, T. Neupert, J. Maciejko, and T. Bzdusek, Hyperbolic non-Abelian semimetal, Phys. Rev. Lett. **132**, 206601 (2024).
[50] Q. Chen, Z. Zhang, H. Qin, A. Bossart, Y. Yang, H. Chen, and R. Fleury, Anomalous and Chern topological waves in hyperbolic networks, Nat. Commun. **15**, 2293 (2024).
[51] L. Huang, L. He, W. Zhang, H. Zhang, D. Liu, X. Feng, F. Liu, K. Cui, Y. Huang, W. Zhang, and X. Zhang, Hyperbolic photonic topological insulators, Nat. Commun. **15**, 1647 (2024).
[52] N. H. Patino, C. Rasmussen, and M. Ruzzene, Hyperbolic space spectral characteristics in a network of mechanical linkages, arXiv:2402.04531.
[53] A. A. Houck, H. E. Türeci, and J. Koch, On-chip quantum simulation with superconducting circuits, Nat. Phys. **8**, 292 (2012).
[54] N. M. Sundaresan, R. Lundgren, G. Zhu, A. V. Gorshkov, and A. A. Houck, Interacting qubit-photon bound states with superconducting circuits, Phys. Rev. X **9**, 011021 (2019).
[55] V. V. Albert, L. I. Glazman, and L. Jiang, Topological properties of linear circuit lattices, Phys. Rev. Lett. **114**, 173902 (2015).
[56] J. Ningyuan, C. Owens, A. Sommer, D. Schuster, and J. Simon, Time- and site-resolved dynamics in a topological circuit, Phys. Rev. X **5**, 021031 (2015).
[57] C. H. Lee, S. Imhof, C. Berger, F. Bayer, J. Brehm, L. W. Molenkamp, T. Kiessling, and R. Thomale, Topolectrical circuits, Commun. Phys. **1**, 1 (2018).
[58] T. Kotwal, F. Moseley, A. Stegmaier, S. Imhof, H. Brand, T. Kießling, R. Thomale, H. Ronellenfitsch, and J. Dunkel, Active topolectrical circuits, Proc. Natl. Acad. Sci. U.S.A. **118**, e2106411118 (2021).
[59] H. Hohmann, T. Hofmann, T. Helbig, S. Imhof, H. Brand, L. K. Upreti, A. Stegmaier, A. Fritzsche, T. Müller, U. Schwingenschlögl, C. H. Lee, M. Greiter, L. W. Molenkamp, T. Kießling, and R. Thomale, Observation of cnoidal wave localization in nonlinear topolectric circuits, Phys. Rev. Res. **5**, L012041 (2023).
[60] T. Ozawa, H. M. Price, A. Amo, N. Goldman, M. Hafezi, L. Lu, M. C. Rechtsman, D. Schuster, J. Simon, O. Zilberberg, and I. Carusotto, Topological photonics, Rev. Mod. Phys. **91**, 015006 (2019).
[61] M. Jalali Mehrabad, S. Mittal, and M. Hafezi, Topological photonics: Fundamental concepts, recent developments, and future directions, Phys. Rev. A **108**, 040101 (2023).
[62] M. Bañados, C. Teitelboim, and J. Zanelli, Black hole in three-dimensional spacetime, Phys. Rev. Lett. **69**, 1849 (1992).
[63] S. Carlip and C. Teitelboim, Aspects of black hole quantum mechanics and thermodynamics in $2+1$ dimensions, Phys. Rev. D **51**, 622 (1995).
[64] E. Keski-Vakkuri, Bulk and boundary dynamics in BTZ black holes, Phys. Rev. D **59**, 104001 (1999).
[65] N. Seiberg, Notes on quantum liouville theory and quantum gravity, Prog. Theor. Phys. Suppl. **102**, 319 (1990).
[66] P. Ginsparg and G. Moore, Lectures on 2D gravity and 2D string theory (TASI 1992), arXiv:hep-th/9304011.
[67] See Supplemental Material at http://link.aps.org/supplemental/10.1103/PhysRevLett.133.061603 for construction of type-II lattices, relation to BTZ geometry, fit procedure, derivation of Eqs. (2), (7), (8), (10), and (11), and electrical circuit simulation.
[68] J. Maldacena and L. Susskind, Cool horizons for entangled black holes, Fortschr. Phys. **61**, 781 (2013).